

3D MEMBRANE THEORY

Carsten Corte

Baustatik – Baudynamik – Numerische Modellierung
Thrasoltstrasse 12, D-10585 Berlin, Tel./Fax +49-(0)30-347 871 78/80

Key words: *Nonlinear Membrane Structures, Deformed State Tensile Force Equilibrium, Finite Element Method, Higher-Order Elements, Hypar Shaped Membranes, Spinnaker Sail Membranes.*

1 Introduction

First industrial tensile roof structures have been constructed about one century ago, Drew [16]. Development on the particular case of tensile membrane structures has been performed since about the 1950s, Frei et al. [1], [5], [6], [7], [8]. Intensive research on computational methods for the design of membrane structures was performed in the 1970s, Weitgespannte Flächentragwerke [9], [10], Zerning [11], Bubner et al. [12], Weitgespannte Flächentragwerke [13], Bubner et al. [14], Brinkmann [15]. Reviews on membrane structures from the beginning until the 20th century are e.g. presented by Drew [16], [20], Hoppe [19], Berger [17], Schock [18]. Nowadays membrane constructions are shown by e.g. Renner [21], Apelmann et al. [22], Goeppert [23], Cremers et al. [24], Seel et al. [25]. Current development of adaptive light weight structures is shown e.g. by Neuhaeuser et al. [26]. Sophisticated numerical methods for to model membrane structures with regard to large deformation have been developed, Trostel [6], Linkwitz et al. [27], Bufler [28], Bletzinger et al. [29], [2], Wuechner et al. [30]. Wuechner [31], Linhard [32] show recent development on form finding for membrane structures. Corte et al. [33], [34], Corte [35] show a force equilibrium based approach on weak [33] and strong [34], [35] coupling of fluid-structure interaction between viscous fluids and elastic structures. Corte [36], [37], [38] shows a consistent approach on fluid-structure interaction for large structural deformation with evaluation [36], [37] and application to a 3D elastic sail structure [38].

2 Analytic force equilibrium

Membrane structures are characterized by tangential in-plane structural tensile stress state, Frei [1]. Thereby membranes match the property that their thickness is orders of magnitude smaller in dimension than surface directions' dimensions are. Therefore out-of-plane stresses are neglected when considering membrane force equilibrium. The undeformed stress free shape of a membrane constitutes a three-dimensional curved surface

that experiences nonzero curvature although its domain. For regions in the membrane where curvature approaches orders near zero curvature, out-of-plane structural membrane stiffness drops drastically and can lead to structural instability within that considered region. For a computational approach the undeformed stress free shape of a considered membrane is here modeled by parametric description: Along the surface expansion of the membrane the two spatial parameters ξ and η are defined. With reference to that defined $\xi - \eta$ coordinate system on the membrane a unique definition of the three-dimensional cartesian coordinates ${}^0\mathbf{x}=[{}^0x(\xi,\eta), {}^0y(\xi,\eta), {}^0z(\xi,\eta)]$ gives the three-dimensional shape of the undeformed stress free membrane. From this undeformed stress free state 0 the membrane may experience spatially distributed displacements that are here introduced with reference to the defined $\xi - \eta$ coordinate system on the membrane as cartesian displacements ${}^{t+\Delta t}\mathbf{u}=[{}^{t+\Delta t}u_x(\xi,\eta), {}^{t+\Delta t}u_y(\xi,\eta), {}^{t+\Delta t}u_z(\xi,\eta)]$ at some equilibrium state $t + \Delta t$. The tensile force equilibrium within the membrane can be expressed with stress and strain definitions that refer to the undeformed stress free state 0 of the membrane (2nd Piola-Kirchhoff stress, Green-Lagrange strain) or with stress and strain definitions that refer to the stress carrying deformed state $t + \Delta t$ (Cauchy stress, Euler-Almansi strain), Bletzinger [2]. Detailed explanation on stress and strain relations depending on the state of reference (state 0, state $t + \Delta t$) is given by Bathe [3]. The membrane structural force equilibrium is here expressed as a spatial integration expression over virtual work contributions in its weak form as

$$\begin{aligned} & \int \int [S_{\xi\xi}(\xi, \eta); S_{\eta\eta}(\xi, \eta); S_{\xi\eta}(\xi, \eta)] \bullet [\delta\epsilon_{\xi\xi}(\xi, \eta); \delta\epsilon_{\eta\eta}(\xi, \eta); \delta\epsilon_{\xi\eta}(\xi, \eta)]^T dA(\xi, \eta) dx_{normal}(\xi, \eta) \\ = & \int \int \rho \cdot [\ddot{u}_x(\xi, \eta); \ddot{u}_y(\xi, \eta); \ddot{u}_z(\xi, \eta)] \bullet [\delta u_x(\xi, \eta); \delta u_y(\xi, \eta); \delta u_z(\xi, \eta)]^T \\ & + [f_x^{ext}(\xi, \eta); f_y^{ext}(\xi, \eta); f_z^{ext}(\xi, \eta)] \bullet [\delta u_x(\xi, \eta); \delta u_y(\xi, \eta); \delta u_z(\xi, \eta)]^T dA(\xi, \eta) dx_{normal}(\xi, \eta) \end{aligned} \quad (1)$$

Here nonlinear membrane stresses are defined as

$$\begin{bmatrix} S_{\xi\xi}(\xi, \eta) \\ S_{\eta\eta}(\xi, \eta) \\ S_{\xi\eta}(\xi, \eta) \end{bmatrix} = \begin{bmatrix} C_{1111} & C_{1122} & C_{1112} \\ C_{2211} & C_{2222} & C_{2212} \\ C_{1211} & C_{1222} & C_{1212} \end{bmatrix} \bullet \begin{bmatrix} \epsilon_{\xi\xi}(\xi, \eta) \\ \epsilon_{\eta\eta}(\xi, \eta) \\ \epsilon_{\xi\eta}(\xi, \eta) \end{bmatrix} \quad (2)$$

where $[(C_{1111}, C_{1122}, C_{1112}); (C_{2211}, C_{2222}, C_{2212}); (C_{1211}, C_{1222}, C_{1212})]$ represents a constant elasticity tensor for linear elastic material ($C_{1111}=C_{2222}=\lambda+2\mu$, $C_{1122}=C_{2211}=\lambda$, $C_{1212}=\mu$, $C_{1112}=C_{2212}=C_{1211}=C_{1222}=0$ for isotropic linear elastic material, λ , μ : Lamé constants). Dependence of the elasticity tensor on the state of reference (state 0 or state $t + \Delta t$) is neglected here (see [3] for further details). Nonlinear membrane strain is defined as

$$\begin{bmatrix} \epsilon_{\xi\xi}(\xi, \eta) \\ \epsilon_{\eta\eta}(\xi, \eta) \\ \epsilon_{\xi\eta}(\xi, \eta) \end{bmatrix} = \begin{bmatrix} \partial u_\xi(\xi, \eta)/\partial x_\xi(\xi, \eta) + \frac{1}{2}\{\partial u_\xi(\xi, \eta)/\partial x_\xi(\xi, \eta)\}^2 + \frac{1}{2}\{\partial u_\eta(\xi, \eta)/\partial x_\xi(\xi, \eta)\}^2 \\ \partial u_\eta(\xi, \eta)/\partial x_\eta(\xi, \eta) + \frac{1}{2}\{\partial u_\xi(\xi, \eta)/\partial x_\eta(\xi, \eta)\}^2 + \frac{1}{2}\{\partial u_\eta(\xi, \eta)/\partial x_\eta(\xi, \eta)\}^2 \\ \{\partial u_\xi(\xi, \eta)/\partial x_\eta(\xi, \eta) + \partial u_\eta(\xi, \eta)/\partial x_\xi(\xi, \eta) \\ + \partial u_\xi(\xi, \eta)/\partial x_\xi(\xi, \eta) \cdot \partial u_\xi(\xi, \eta)/\partial x_\eta(\xi, \eta) \\ + \partial u_\eta(\xi, \eta)/\partial x_\xi(\xi, \eta) \cdot \partial u_\eta(\xi, \eta)/\partial x_\eta(\xi, \eta)\} \end{bmatrix} \quad (3)$$

Along the ξ - η parameter coordinate system on the undeformed initial geometric membrane surface appropriate surface tangential vectors ${}^0\mathbf{g}_\xi(\xi, \eta) = \partial[{}^0\mathbf{x}(\xi, \eta) + 0, {}^0\mathbf{y}(\xi, \eta) + 0, {}^0\mathbf{z}(\xi, \eta) + 0] / \partial\xi$ and ${}^0\mathbf{g}_\eta(\xi, \eta) = \partial[{}^0\mathbf{x}(\xi, \eta) + 0, {}^0\mathbf{y}(\xi, \eta) + 0, {}^0\mathbf{z}(\xi, \eta) + 0] / \partial\eta$ as well as surface normal vector ${}^0\mathbf{g}_{normal}(\xi, \eta) = {}^0\mathbf{g}_\xi(\xi, \eta) \times {}^0\mathbf{g}_\eta(\xi, \eta)$ with reference to the undeformed stress free state 0 and ${}^{t+\Delta t}\mathbf{g}_\xi(\xi, \eta) = \partial[{}^0\mathbf{x}(\xi, \eta) + {}^{t+\Delta t}\mathbf{u}_x(\xi, \eta), {}^0\mathbf{y}(\xi, \eta) + {}^{t+\Delta t}\mathbf{u}_y(\xi, \eta), {}^0\mathbf{z}(\xi, \eta) + {}^{t+\Delta t}\mathbf{u}_z(\xi, \eta)] / \partial\xi$ and ${}^{t+\Delta t}\mathbf{g}_\eta(\xi, \eta) = \partial[{}^0\mathbf{x}(\xi, \eta) + {}^{t+\Delta t}\mathbf{u}_x(\xi, \eta), {}^0\mathbf{y}(\xi, \eta) + {}^{t+\Delta t}\mathbf{u}_y(\xi, \eta), {}^0\mathbf{z}(\xi, \eta) + {}^{t+\Delta t}\mathbf{u}_z(\xi, \eta)] / \partial\eta$ as well as surface normal vector ${}^{t+\Delta t}\mathbf{g}_{normal}(\xi, \eta) = {}^{t+\Delta t}\mathbf{g}_\xi(\xi, \eta) \times {}^{t+\Delta t}\mathbf{g}_\eta(\xi, \eta)$ with reference to the deformed state $t + \Delta t$ are unique.

With unique tangential vectors as above the displacements in local ξ - and local η -direction are thereby defined as ${}^{t+\Delta t}\mathbf{u}_\xi(\xi, \eta) = {}^{t+\Delta t}\mathbf{u}(\xi, \eta) \bullet {}^0\mathbf{g}_\xi(\xi, \eta)$ and ${}^{t+\Delta t}\mathbf{u}_\eta(\xi, \eta) = {}^{t+\Delta t}\mathbf{u}(\xi, \eta) \bullet {}^0\mathbf{g}_\eta(\xi, \eta)$ as well as ${}^{t+\Delta t}\mathbf{u}_\xi(\xi, \eta) = {}^{t+\Delta t}\mathbf{u}(\xi, \eta) \bullet {}^{t+\Delta t}\mathbf{g}_\xi(\xi, \eta)$ and ${}^{t+\Delta t}\mathbf{u}_\eta(\xi, \eta) = {}^{t+\Delta t}\mathbf{u}(\xi, \eta) \bullet {}^{t+\Delta t}\mathbf{g}_\eta(\xi, \eta)$ with respect to the undeformed stress free state 0 and the deformed state $t + \Delta t$ of the membrane, respectively. Spatial coordinates of the membrane in local ξ - and local η -direction are defined as ${}^{t+\Delta t}\mathbf{x}_\xi(\xi, \eta) = {}^0\mathbf{x}(\xi, \eta) \bullet {}^0\mathbf{g}_\xi(\xi, \eta)$ and ${}^{t+\Delta t}\mathbf{x}_\eta(\xi, \eta) = {}^0\mathbf{x}(\xi, \eta) \bullet {}^0\mathbf{g}_\eta(\xi, \eta)$ as well as ${}^{t+\Delta t}\mathbf{x}_\xi(\xi, \eta) = {}^0\mathbf{x}(\xi, \eta) \bullet {}^{t+\Delta t}\mathbf{g}_\xi(\xi, \eta)$ and ${}^{t+\Delta t}\mathbf{x}_\eta(\xi, \eta) = {}^0\mathbf{x}(\xi, \eta) \bullet {}^{t+\Delta t}\mathbf{g}_\eta(\xi, \eta)$, respectively. Concerning the virtual work expression of the membrane structural force equilibrium in equation (1) linearized virtual membrane strain is defined as

$$\begin{aligned} & [\delta\epsilon_{\xi\xi}(\xi, \eta); \delta\epsilon_{\eta\eta}(\xi, \eta); \delta\epsilon_{\xi\eta}(\xi, \eta)]^T \\ = & [\partial\delta u_\xi(\xi, \eta) / \partial x_\xi(\xi, \eta); \partial\delta u_\eta(\xi, \eta) / \partial x_\eta(\xi, \eta); \partial\delta u_\xi(\xi, \eta) / \partial x_\eta(\xi, \eta) + \partial\delta u_\eta(\xi, \eta) / \partial x_\xi(\xi, \eta)]^T \end{aligned} \quad (4)$$

with virtual displacements $\delta_0^{t+\Delta t}u_\xi(\xi, \eta)$, $\delta_0^{t+\Delta t}u_\eta(\xi, \eta)$ and $\delta_{t+\Delta t}^{t+\Delta t}u_\xi(\xi, \eta)$, $\delta_{t+\Delta t}^{t+\Delta t}u_\eta(\xi, \eta)$ according to definitions of ${}^{t+\Delta t}u_\xi(\xi, \eta)$, ${}^{t+\Delta t}u_\eta(\xi, \eta)$ and ${}^{t+\Delta t}u_\xi(\xi, \eta)$, ${}^{t+\Delta t}u_\eta(\xi, \eta)$ above appropriately.

The analytic form of the membrane area differential is given by $d^0A(\xi, \eta) = {}^0\mathbf{g}_\xi(\xi, \eta) \times {}^0\mathbf{g}_\eta(\xi, \eta) d\xi d\eta$ and $d^{t+\Delta t}A(\xi, \eta) = {}^{t+\Delta t}\mathbf{g}_\xi(\xi, \eta) \times {}^{t+\Delta t}\mathbf{g}_\eta(\xi, \eta) d\xi d\eta$, respectively. Membrane thickness ${}^0x_{normal}(\xi, \eta)$ and ${}^{t+\Delta t}x_{normal}(\xi, \eta)$, respectively, may vary along the membrane but is to fulfil the requirement that it is neglectably small compared with the membrane dimensions in membrane tangential directions.

With regard to equation (1) that describes the weak form of the membrane force equilibrium it concludes that the partial derivatives of the sum of virtual work contributions with respect to the unknown displacement result as zero as a property of the (analytic) membrane force equilibrium for each position (ξ, η) of the considered membrane; with this demand it results that (compare with equation (1))

$$\begin{aligned}
 & \int \int \begin{bmatrix} C_{1111} & C_{1122} & C_{1112} \\ C_{2211} & C_{2222} & C_{2212} \\ C_{1211} & C_{1222} & C_{1212} \end{bmatrix} \bullet [[\epsilon_{\xi\xi}(\xi, \eta); \epsilon_{\eta\eta}(\xi, \eta); \epsilon_{\xi\eta}(\xi, \eta)]^T \\
 & + \partial[\epsilon_{\xi\xi}(\xi, \eta); \epsilon_{\eta\eta}(\xi, \eta); \epsilon_{\xi\eta}(\xi, \eta)]^T / \partial u_x(\xi, \eta) \cdot \Delta u_x(\xi, \eta) \\
 & + \partial[\epsilon_{\xi\xi}(\xi, \eta); \epsilon_{\eta\eta}(\xi, \eta); \epsilon_{\xi\eta}(\xi, \eta)]^T / \partial u_y(\xi, \eta) \cdot \Delta u_y(\xi, \eta) \\
 & + \partial[\epsilon_{\xi\xi}(\xi, \eta); \epsilon_{\eta\eta}(\xi, \eta); \epsilon_{\xi\eta}(\xi, \eta)]^T / \partial u_z(\xi, \eta) \cdot \Delta u_z(\xi, \eta) \\
 & \bullet [\delta\epsilon_{\xi\xi}(\xi, \eta); \delta\epsilon_{\eta\eta}(\xi, \eta); \delta\epsilon_{\xi\eta}(\xi, \eta)]^T dA(\xi, \eta) dx_{normal}(\xi, \eta) \\
 = & \int \int [\rho[\ddot{u}_x(\xi, \eta); \ddot{u}_y(\xi, \eta); \ddot{u}_z(\xi, \eta)] + [f_x^{ext}(\xi, \eta); f_y^{ext}(\xi, \eta); f_z^{ext}(\xi, \eta)] \\
 & + \partial\{ \rho[\ddot{u}_x(\xi, \eta); \ddot{u}_y(\xi, \eta); \ddot{u}_z(\xi, \eta)] + [f_x^{ext}(\xi, \eta); f_y^{ext}(\xi, \eta); f_z^{ext}(\xi, \eta)]\} / \partial u_x(\xi, \eta) \cdot \Delta u_x(\xi, \eta) \\
 & + \partial\{ \rho[\ddot{u}_x(\xi, \eta); \ddot{u}_y(\xi, \eta); \ddot{u}_z(\xi, \eta)] + [f_x^{ext}(\xi, \eta); f_y^{ext}(\xi, \eta); f_z^{ext}(\xi, \eta)]\} / \partial u_y(\xi, \eta) \cdot \Delta u_y(\xi, \eta) \\
 & + \partial\{ \rho[\ddot{u}_x(\xi, \eta); \ddot{u}_y(\xi, \eta); \ddot{u}_z(\xi, \eta)] + [f_x^{ext}(\xi, \eta); f_y^{ext}(\xi, \eta); f_z^{ext}(\xi, \eta)]\} / \partial u_z(\xi, \eta) \cdot \Delta u_z(\xi, \eta)] \\
 & \bullet [\delta u_x(\xi, \eta); \delta u_y(\xi, \eta); \delta u_z(\xi, \eta)]^T dA(\xi, \eta) dx_{normal}(\xi, \eta) \tag{5}
 \end{aligned}$$

with $\Delta u_x(\xi, \eta)$, $\Delta u_y(\xi, \eta)$ and $\Delta u_z(\xi, \eta)$ being the cartesian components of the total differential of the displacement at (ξ, η) in deformed state $t + \Delta t$. Thus equation (5) expresses the analytic form of the membrane force equilibrium equivalently to equation (1).

3 Discretization

Spatial discretization is performed by 9-node-4-corner elements and quadratic polynomials for interpolation of translational displacements within each element, Bathe [3]. Time discretization is performed by application of the HHT- α method, Hilber et al. [4].

For spatial discretization within a 9-node-4-corner element and quadratic polynomials for interpolation of translational displacements within the respective element the appropriate interpolation functions

$$\begin{aligned}
 N_1(\xi_e, \eta_e) &= \frac{1}{4}(1 - \xi_e)(1 - \eta_e) & -\frac{1}{4}(1 - \xi_e^2)(1 - \eta_e) & -\frac{1}{4}(1 - \xi_e)(1 - \eta_e^2) & +\frac{1}{4}(1 - \xi_e^2)(1 - \eta_e^2) \\
 N_2(\xi_e, \eta_e) &= \frac{1}{4}(1 + \xi_e)(1 - \eta_e) & -\frac{1}{4}(1 - \xi_e^2)(1 - \eta_e) & -\frac{1}{4}(1 + \xi_e)(1 - \eta_e^2) & +\frac{1}{4}(1 - \xi_e^2)(1 - \eta_e^2) \\
 N_3(\xi_e, \eta_e) &= \frac{1}{4}(1 + \xi_e)(1 + \eta_e) & -\frac{1}{4}(1 - \xi_e^2)(1 + \eta_e) & -\frac{1}{4}(1 + \xi_e)(1 - \eta_e^2) & +\frac{1}{4}(1 - \xi_e^2)(1 - \eta_e^2) \\
 N_4(\xi_e, \eta_e) &= \frac{1}{4}(1 - \xi_e)(1 + \eta_e) & -\frac{1}{4}(1 - \xi_e^2)(1 + \eta_e) & -\frac{1}{4}(1 - \xi_e)(1 - \eta_e^2) & +\frac{1}{4}(1 - \xi_e^2)(1 - \eta_e^2) \\
 N_5(\xi_e, \eta_e) &= & \frac{1}{2}(1 - \xi_e^2)(1 - \eta_e) & & -\frac{1}{2}(1 - \xi_e^2)(1 - \eta_e^2) \\
 N_6(\xi_e, \eta_e) &= & & \frac{1}{2}(1 + \xi_e)(1 - \eta_e^2) & -\frac{1}{2}(1 - \xi_e^2)(1 - \eta_e^2) \\
 N_7(\xi_e, \eta_e) &= & \frac{1}{2}(1 - \xi_e^2)(1 + \eta_e) & & -\frac{1}{2}(1 - \xi_e^2)(1 - \eta_e^2) \\
 N_8(\xi_e, \eta_e) &= & & \frac{1}{2}(1 - \xi_e)(1 - \eta_e^2) & -\frac{1}{2}(1 - \xi_e^2)(1 - \eta_e^2) \\
 N_9(\xi_e, \eta_e) &= & & & (1 - \xi_e^2)(1 - \eta_e^2)
 \end{aligned}$$

are shown (compare with [3]); ξ_e and η_e are here element specific parameter coordinates ($\xi_e = -1 \dots 1$, $\eta_e = -1 \dots 1$). Spatial derivatives $\partial N_1(\xi_e, \eta_e) / \partial \xi \dots \partial N_9(\xi_e, \eta_e) / \partial \xi$, $\partial N_1(\xi_e, \eta_e) / \partial \eta \dots \partial N_9(\xi_e, \eta_e) / \partial \eta$, $\partial \partial N_1(\xi_e, \eta_e) / \partial \xi \partial \xi \dots \partial \partial N_9(\xi_e, \eta_e) / \partial \xi \partial \xi$, $\partial \partial N_1(\xi_e, \eta_e) / \partial \eta \partial \eta \dots \partial \partial N_9(\xi_e, \eta_e) / \partial \eta \partial \eta$, $\partial \partial N_1(\xi_e, \eta_e) / \partial \xi \partial \eta \dots \partial \partial N_9(\xi_e, \eta_e) / \partial \xi \partial \eta$, $\partial \partial N_1(\xi_e, \eta_e) / \partial \eta \partial \xi \dots \partial \partial N_9(\xi_e, \eta_e) / \partial \eta \partial \xi$ (ξ, η : parameter coordinates for membrane shape definition) follow

| Node | x | y | z | u_x | u_y | u_z | Gausspoint | ξ | η | Gaussweight | u_x | u_y | u_z |
|------|----|----|---|-------|-------|-------|------------|------------|------------|------------------------------|-------|-------|-------|
| 1 | -1 | -1 | 0 | 1 | 1 | 1 | 1 | -0.7746... | -0.7746... | $\frac{25}{81} \approx 0.31$ | 0.84 | 0.84 | 0.84 |
| 2 | 1 | -1 | 0 | 1 | 1 | 1 | 2 | -0.7746... | 0.0000... | $\frac{40}{81} \approx 0.49$ | 0.60 | 0.60 | 0.60 |
| 3 | 1 | 1 | 0 | 1 | 1 | 1 | 3 | -0.7746... | 0.7746... | $\frac{25}{81} \approx 0.31$ | 0.84 | 0.84 | 0.84 |
| 4 | -1 | 1 | 0 | 1 | 1 | 1 | 4 | 0.0000... | -0.7746... | $\frac{40}{81} \approx 0.49$ | 0.60 | 0.60 | 0.60 |
| 5 | 0 | -1 | 0 | 1 | 1 | 1 | 5 | 0.0000... | 0.0000... | $\frac{64}{81} \approx 0.79$ | 0.00 | 0.00 | 0.00 |
| 6 | 1 | 0 | 0 | 1 | 1 | 1 | 6 | 0.0000... | 0.7746... | $\frac{40}{81} \approx 0.49$ | 0.60 | 0.60 | 0.60 |
| 7 | 0 | 1 | 0 | 1 | 1 | 1 | 7 | 0.7746... | -0.7746... | $\frac{25}{81} \approx 0.31$ | 0.84 | 0.84 | 0.84 |
| 8 | -1 | 0 | 0 | 1 | 1 | 1 | 8 | 0.7746... | 0.0000... | $\frac{40}{81} \approx 0.49$ | 0.60 | 0.60 | 0.60 |
| 9 | 0 | 0 | 0 | 0 | 0 | 0 | 9 | 0.7746... | 0.7746... | $\frac{25}{81} \approx 0.31$ | 0.84 | 0.84 | 0.84 |

Table 1: unit element nodes with unit nodal displacement and Gausspoint displacement

uniquely.

For time discretization the HHT- α method [4] applies

$$\begin{aligned}
{}^{t+\Delta t}\ddot{\mathbf{u}}(\xi, \eta) &= 1/(\beta\Delta t^2)[{}^{t+\Delta t}\mathbf{u}(\xi, \eta) - {}^t\mathbf{u}(\xi, \eta) - \Delta t{}^t\dot{\mathbf{u}}(\xi, \eta) - \Delta t^2(0.5 - \beta){}^t\ddot{\mathbf{u}}(\xi, \eta)] \\
{}^{t+\Delta t}\dot{\mathbf{u}}(\xi, \eta) &= {}^t\dot{\mathbf{u}}(\xi, \eta) + \Delta t[(1 - \gamma){}^t\ddot{\mathbf{u}}(\xi, \eta) + \gamma{}^{t+\Delta t}\ddot{\mathbf{u}}(\xi, \eta)]
\end{aligned} \tag{6}$$

to express time discrete acceleration and velocity for a discrete time interval $[t; t + \Delta t]$ ($\alpha \in [-\frac{1}{3}; 0]$, $\beta = \frac{(1-\alpha)^2}{4}$ and $\gamma = \frac{1}{2} - \alpha$: time integration parameters).

Introduction of spatial discretization and time discretization into equation (5) leads to the discrete nonlinear equation system that gives the consistent discrete description of the stated problem. The discrete nonlinear equation system can be solved in an iterative manner to eventually obtain the spatially discrete and time discrete unknown displacements $[{}^{t+\Delta t}\mathbf{u}_x^k(\xi, \eta), {}^{t+\Delta t}\mathbf{u}_y^k(\xi, \eta), {}^{t+\Delta t}\mathbf{u}_z^k(\xi, \eta)]$, $k = 1 \dots N_k$ (N_k : number of discrete nodes in the appropriate finite element discretization). Spatial integration over discrete surface elements with quadratic polynomials for interpolation of translational displacement can be performed exactly by Gausspoint integration.

4 Evaluation

Evaluation of the discrete system for the case of even in-plane load and for the case of out-of-plane load on the unit 9-node-4-corner element is performed. Appropriate stiffness and mass matrix coefficients for the unit 9-node-4-corner element are shown. In-plane displacement as well as out-of-plane displacement is assessed. The setup of the different evaluation cases is illustrated in figure 1.

4.1 Boundary displacement: Interpolation

The unit 9-node-4-corner element with nodal coordinates as in table (1) is exposed to nodal boundary displacement (table (1), central node undisplaced). Spatial integration is performed by 3×3 Gausspoints with Gausspoint coordinates as in table (1). Interpolated displacement values at the appropriate Gausspoint coordinates are shown in table (1).

| Node | x | y | z | u_x | u_y | u_z |
|------|----|----|---|-------|-------|-------|
| 1 | -1 | -1 | 0 | -1 | -1 | 0 |
| 2 | 1 | -1 | 0 | 1 | -1 | 0 |
| 3 | 1 | 1 | 0 | 1 | 1 | 0 |
| 4 | -1 | 1 | 0 | -1 | 1 | 0 |
| 5 | 0 | -1 | 0 | 0 | -1 | 0 |
| 6 | 1 | 0 | 0 | 1 | 0 | 0 |
| 7 | 0 | 1 | 0 | 0 | 1 | 0 |
| 8 | -1 | 0 | 0 | -1 | 0 | 0 |
| 9 | 0 | 0 | 0 | 0 | 0 | 0 |

Table 2: unit element nodes with ± 1.0 nodal displacement

4.2 In-plane boundary displacement: Stiffness and mass coefficients

The unit 9-node-4-corner element with nodal coordinates as in table (2) is exposed to nodal boundary displacement as in table (2) with undisplaced central node. Spatial integration is performed by 3×3 Gausspoints with Gausspoint coordinates as in table (1). Material stiffness parameters are Lamé constants $\lambda=1$ and $\mu=1$. Material density is $\rho=1000$. Membrane thickness is $h_z=1$. As an excerpt of the stiffness matrix of the discrete system of the unit 9-node-4-corner element the displacement-appropriate stiffness matrix coefficients are shown in table (3) for influence of nodal x-displacement on nodal inner elastic x-forces. Analogous an excerpt of the stiffness matrix of the discrete system of the unit 9-node-4-corner element is shown in table (4) for influence of nodal y-displacement on nodal inner elastic y-forces. Since nodal displacement in z-direction (see table (2)) is identical to zero the appropriate stiffness matrix coefficients for influence of nodal z-displacement on any nodal inner elastic forces for the considered unit 9-node-4-corner element (that is positioned even in the x-y-plane) are identical zero which is not any further listed here.

It is commented here that due to the large nodal displacements compared with the element dimensions (see table (2)) high amounts of non-symmetry in the stiffness matrix coefficients appear for coefficients in tables (3) and (4). This non-symmetry appears due to the application of quadratic interpolation function and their different spatial derivatives within the considered (unit) 9-node-4-corner element. Consideration of the arrangement of the different nodes in the 9-node-4-corner element makes obvious that there appears a regular pattern within the non-symmetry of the stiffness coefficients.

Displacement-independent mass matrix coefficients for the discrete system of the unit 9-node-4-corner element are shown in table (5) that are valid for influence of nodal x-acceleration on nodal inertia x-forces as well as for nodal y-acceleration on nodal inertia y-forces and for nodal z-acceleration on nodal inertia z-forces.

4.3 In-plane boundary displacement: Displacement dependence of stiffness coefficients

Regarding the non-symmetry in the stiffness matrix coefficients that appears for boundary displacement as shown in table (2) and that can be seen in tables (3) and (4) the amount

of non-symmetry in the appropriate stiffness matrix coefficients decreases for smaller boundary displacement compared with the element dimensions. This is evaluated for ± 0.1 nodal boundary displacement as in table (6), for ± 0.01 nodal boundary displacement as in table (7) and for ± 0.001 nodal boundary displacement as in table (8). Appropriate excerpts of the stiffness matrices for influence of nodal x-displacement on nodal inner elastic x-forces are shown in tables (9), (10) and (11). The percentage of non-symmetry in the stiffness matrix coefficients is of the same order as the relation between nodal boundary displacement and element dimensions and decreases approximately linearly with the nodal boundary displacement.

4.4 In-plane boundary forces: Free corners, fixed edge midpoints

For the four corner nodes being exposed to outward-directed external forces of amount ± 0.01 in x- and in y-direction, where edge midpoint nodes and central node are fixed in displacement, the static solution in corner displacement is given with respect to the appropriate equilibrium iteration in table (12) until convergence is achieved; material stiffness parameters are $\lambda=1$ and $\mu=1$, membrane thickness is $h_z=1$. The static displacement is converged after four equilibrium iterations and shows outward displacement of the four corner nodes of amount ± 0.005914 in both x- and y-direction.

4.5 In-plane boundary forces: Free corners, free edge midpoints

For the four corner nodes being exposed to outward-directed external forces of amount ± 0.01 in x- and in y-direction and for the four edge midpoint nodes being exposed to outward-directed external forces of amount ± 0.01 in x- and in y-direction, respectively, where the tangential displacement of the four edge midpoint nodes and the displacement of the central node are fixed, the static solution in corner displacement is given with respect to the appropriate equilibrium iteration in table (13) until convergence is achieved; material stiffness parameters are $\lambda=1$ and $\mu=1$, membrane thickness is $h_z=1$. The static displacement is converged after four equilibrium iterations and shows outward displacement of the four corner nodes of amount ± 0.006330 in both x- and y-direction and outward normal displacement of the four edge midpoint nodes of amount ± 0.002772 . Since the edge midpoint nodes can displace in normal direction to the element edges appropriately the outward corner displacement of amount ± 0.006330 in both x- and y-direction is larger in magnitude than for the case of fixed edge midpoint nodes (where outward corner displacement is of amount ± 0.005914 in both x- and y-direction as above, see 4.4).

In table (14) the static solution for outward-directed external forces of amount ± 0.01 in x- and in y-direction on the four corner nodes and outward-directed external forces of amount ± 0.01 in x- and in y-direction, respectively, where the tangential displacement of the four edge midpoint nodes and the displacement of the central node are fixed, on the four edge midpoint nodes is given in corner and edge midpoint displacement with respect to the appropriate equilibrium iteration until convergence is achieved, where here material stiffness parameters are $\lambda=1$ and $\mu=1$ and membrane thickness is $h_z=0.1$, i.e. membrane thickness is 10 times smaller than for the system shown in table (13). Since the system shown in table (14) has smaller stiffness than the system shown in table (13) the

converged displacement solution is obtained after more than four iterations (compare with table (13)). Corner nodes' displacement shows converged solution of amount ± 0.047872 in both x- and y-direction, and edge midpoint nodes' displacement shows converged solution of amount ± 0.020507 in normal direction to the edges. Comparing systems in tables (13) and (14), where membrane thickness relation is $1/0.1=10/1$, it shows that corner displacement relation is $0.006330/0.047872=1/7.563>1/10$ and that edge midpoint displacement relation is $0.002772/0.020507=1/7.398>1/10$, which indicates the nonlinearly (super-linearly) increasing geometric stiffness of the membrane and thereby nonlinearly (sub-linearly) increasing displacements for linearly decreasing membrane thickness.

4.6 Out-of-plane central force: Fixed corners, free edge midpoints

For to evaluate the membrane reaction on out-of-plane load, the unit 9-node-4-corner element is exposed to a normal out-of-plane single force of amount 10^{-5} on its central node. Material stiffness parameters are $\lambda=1$ and $\mu=1$, membrane thickness is $h_z=0.001$, nodal coordinates are shown in table (15). Since out-of-plane stiffness of membranes is zero for completely even membranes, for the initial stress free shape of the membrane the central node is lowered out-of-plane compared with the corner nodes and edge midpoint nodes; this induces an initial nonzero stiffness of the membrane in out-of-plane, i.e. normal direction of the membrane. The out-of-plane coordinate of the central node is considered to be 0.01 (case 1), 0.001 (case 2), 0.0001 (case 3) and 0.00001 (case 4), respectively. The converged displacement solution for cases 1 to 4 is shown in table (15). For out-of-plane coordinate 0.01 of the central node (case 1) converged out-of-plane displacement of the central node is 0.020794; for cases 2, 3 and 4 (out-of-plane coordinate 0.001, 0.0001, 0.00001 of the central node, respectively) converged out-of-plane displacement of the central node is 0.105609499, 0.106090596 and 0.106138805, respectively. Comparison of out-of-plane displacement of the central node 0.020794 for case 1 with out-of-plane displacement of the central node 0.105609499 for case 2, 0.106090596 for case 3 and 0.106138805 for case 4 shows that for case 1 still material stiffness acts in out-of-plane direction whereas for cases 2, 3 and 4 (since out-of-plane displacement of the central node for these three cases is almost the same) only geometric stiffness acts in out-of-plane direction; this indicates the nonlinear geometric stiffness as a property of the membrane that is represented by the applied membrane element type with the applied numeric approach.

4.7 Out-of-plane eigenload: Fixed corners, fixed edges

A quadratic membrane of edge length 2 is considered. Material stiffness parameters are $\lambda=10^{10}$ and $\mu=10^{10}$ (equivalent to modulus of elasticity $E=2.5 \cdot 10^{10}$ and Poisson ratio $\nu=0.25$), material density is $\rho=1000$, membrane thickness is $h_z=0.001$, gravity is $g_z=10$. The undeformed stress free shape of the membrane is defined by the quadratic out-of-plane shape $z(x,y)=0.001 \cdot (x-1)(x+1)(y-1)(y+1)$. The considered membrane in x-y-plane is exposed to eigenload in out-of-plane z-direction. The membrane is supported in out-of-plane z-direction along its edges. Since the membrane has uniquely oriented curvature throughout its domain the membrane is completely fixed in x- and y-displacement to

avoid any in-plane x-y-displacement. For comparison of different discretization levels the membrane is regularly meshed with one quadratic 9-node-4-corner element (case 1, 9 nodes), with 2×2 quadratic 9-node-4-corner elements (case 2, 25 nodes) and with 8×8 quadratic 9-node-4-corner elements (case 3, 289 nodes). Appropriate converged solutions for out-of-plane z-displacement are shown in table (16) for cases 1, 2 and 3. Comparison shows that nodal z-displacement is largest for the center of the membrane (node 9, 0.00324 for case 1, 0.00303 for case 2, 0.00296 for case 3). Node 289 near the membrane center has z-displacement 0.00278, so slightly less than for the center itself. Node 18 between membrane center and membrane edge center has z-displacement of 0.00181 (case 2) and 0.00171 (case 3), respectively. Node 22 between membrane center and membrane corner has z-displacement of 0.00155 (case 2) and 0.00148 (case 3), respectively. Out-of-plane z-displacement is largest for the membrane center, followed by second-largest z-displacement in the vicinity of the membrane and even smaller z-displacement towards the membrane edges and membrane corners. As the above definition $z(x,y)$ of the undeformed stress free out-of-plane shape of the membrane indicates the slope of the membrane is zero in the membrane center. The zero slope in the membrane center induces the smallest geometric stiffness with respect to out-of-plane eigenload in z-direction and therefore the largest out-of-plane z-displacement within the membrane. The fact that nodal displacement decreases with increasing number of elements for discretization indicates that refined consideration of the quadratic out-of-plane shape in z-direction (for 2×2 elements and even more for 8×8 elements) leads to a higher stiffness of the membrane than the one element discretization where the quadratic out-of-plane shape in z-direction is considered only by one out-of-plane node (the central node 9).

In figure 2 the out-of-plane z-displacement distribution for case 3 (8×8 elements) is shown. As well the appropriate distribution of normal stresses $S_{\xi\xi}(\xi,\eta)$ and $S_{\eta\eta}(\xi,\eta)$ and shear stress $S_{\xi\eta}(\xi,\eta)$ are shown in figure 2 where computation of stress values is performed at the 3×3 Gausspoints of each element. Around the center of the membrane (node 9 and vicinity) it becomes obvious that the membrane is in compression and no tensile stresses appear at the center of the membrane and its vicinity. Normal stresses $S_{\xi\xi}(\xi,\eta)$ and $S_{\eta\eta}(\xi,\eta)$ are maximum around the edge midpoints where maximum normal tensile stresses act orthogonal to the appropriate edges; due to high tensile strain around the edge midpoints directed towards the membrane center accordingly slight normal stress parallel to the edges appears. Along the diagonals of the membrane in the region of tensile normal stress the shear stress $S_{\xi\eta}(\xi,\eta)$ shows maximum magnitude. To indicate where the membrane experiences compression appropriate pseudo-stress fields for normal stresses $S_{\xi\xi}^{pseudo}(\xi,\eta)$ and $S_{\eta\eta}^{pseudo}(\xi,\eta)$ and for shear stress $S_{\xi\eta}^{pseudo}(\xi,\eta)$ are determined by application of a pseudo-elasticity tensor that shows constant stiffness for both tension and compression; appropriate pseudo-stress distributions are shown in figure 2.

5 Applications

Application of the presented numeric approach is performed on the example of a Hypar shaped membrane exposed to out-of-plane work load and to a spinnaker sail membrane exposed to horizontal pressure load.

| Node | 1 | 2 | 3 | 4 | 5 | 6 | 7 | 8 | 9 |
|------|--------|--------|--------|--------|--------|--------|--------|--------|---------|
| 1 | 31.46 | 4.73 | -1.46 | -2.73 | -27.86 | 3.73 | 6.53 | -3.73 | -10.66 |
| 2 | sym | 31.46 | -2.73 | -1.46 | -27.86 | -3.73 | 6.53 | 3.73 | -10.66 |
| 3 | sym | sym | 31.46 | 4.73 | 6.53 | -3.73 | -27.86 | 3.73 | -10.66 |
| 4 | sym | sym | sym | 31.46 | 6.53 | 3.73 | -27.86 | -3.73 | -10.66 |
| 5 | -19.86 | -19.86 | sym | sym | 65.06 | -18.66 | -11.73 | -18.66 | 10.66 |
| 6 | 4.13 | 0.66 | 0.66 | 4.13 | -7.46 | 98.66 | 7.46 | 19.73 | -113.06 |
| 7 | sym | sym | -19.86 | -19.86 | sym | -18.66 | 65.06 | -18.66 | 10.66 |
| 8 | 0.66 | 4.13 | 4.13 | 0.66 | -7.46 | sym | -7.46 | 98.66 | -113.06 |
| 9 | -23.46 | -23.46 | -23.46 | -23.46 | 4.20 | -81.06 | 4.26 | -81.06 | 247.46 |

Table 3: unit element stiffness coefficients k_{xx} for nodal coordinates and ± 1.0 displacements as in table (2), 3×3 Gausspoints, material stiffness parameters $\lambda = \mu = 1$ and element thickness $h_Z = 1$

| Node | 1 | 2 | 3 | 4 | 5 | 6 | 7 | 8 | 9 |
|------|--------|--------|--------|--------|--------|--------|--------|--------|---------|
| 1 | 31.46 | -2.73 | -1.46 | -4.73 | -3.73 | 6.53 | 3.73 | -27.86 | -10.66 |
| 2 | sym | 31.46 | 4.73 | -1.46 | -3.73 | -27.86 | 3.73 | 6.53 | -10.66 |
| 3 | sym | sym | 31.46 | -2.73 | 3.73 | -27.86 | -3.73 | 6.53 | -10.66 |
| 4 | sym | sym | sym | 31.46 | 3.73 | 6.53 | -3.73 | -27.86 | -10.66 |
| 5 | 0.66 | 0.66 | 4.13 | 4.13 | 98.66 | -7.46 | 19.73 | -7.46 | -113.06 |
| 6 | sym | -19.86 | -19.86 | sym | -18.66 | 65.06 | -18.66 | -11.73 | 10.66 |
| 7 | 4.13 | 4.13 | 0.66 | 0.66 | sym | -7.46 | 98.06 | -7.46 | -113.06 |
| 8 | -19.86 | sym | -19.86 | -19.86 | -18.66 | sym | -18.66 | 65.06 | 10.66 |
| 9 | -23.46 | -23.46 | -23.46 | -23.46 | -81.06 | 4.26 | -81.06 | 4.26 | 247.46 |

Table 4: unit element stiffness coefficients k_{yy} for nodal coordinates and ± 1.0 displacements as in table (2), 3×3 Gausspoints, material stiffness parameters $\lambda = \mu = 1$ and element thickness $h_Z = 1$

| Node | 1 | 2 | 3 | 4 | 5 | 6 | 7 | 8 | 9 |
|------|-------|--------|--------|--------|--------|--------|--------|--------|---------|
| 1 | 71.11 | -17.77 | 4.44 | -17.77 | 35.55 | -8.88 | -8.88 | 35.55 | 17.77 |
| 2 | sym | 71.11 | -17.11 | 4.44 | 35.55 | 35.55 | -8.88 | -8.88 | 17.77 |
| 3 | sym | sym | 71.11 | -17.77 | -8.88 | 35.55 | 35.55 | -8.88 | 17.77 |
| 4 | sym | sym | sym | 71.11 | -8.88 | -8.88 | 35.55 | 35.55 | 17.77 |
| 5 | sym | sym | sym | sym | 284.44 | 17.77 | -71.11 | 17.77 | 142.22 |
| 6 | sym | sym | sym | sym | sym | 284.44 | 17.77 | -71.11 | 142.22 |
| 7 | sym | sym | sym | sym | sym | sym | 284.44 | 17.77 | 142.22 |
| 8 | sym | sym | sym | sym | sym | sym | sym | 284.44 | 142.22 |
| 9 | sym | sym | sym | sym | sym | sym | sym | sym | 1137.77 |

Table 5: unit element mass coefficients m_{xx} , m_{yy} and m_{zz} , respectively, for nodal coordinates as in table (2), 3×3 Gausspoints, material density $\rho = 1000$ and element thickness $h_Z = 1$

| Node | x | y | z | u_x | u_y | u_z |
|------|----|----|---|-------|-------|-------|
| 1 | -1 | -1 | 0 | -0.1 | -0.1 | 0 |
| 2 | 1 | -1 | 0 | 0.1 | -0.1 | 0 |
| 3 | 1 | 1 | 0 | 0.1 | 0.1 | 0 |
| 4 | -1 | 1 | 0 | -0.1 | 0.1 | 0 |
| 5 | 0 | -1 | 0 | 0.0 | -0.1 | 0 |
| 6 | 1 | 0 | 0 | 0.1 | 0.0 | 0 |
| 7 | 0 | 1 | 0 | 0.0 | 0.1 | 0 |
| 8 | -1 | 0 | 0 | -0.1 | 0.0 | 0 |
| 9 | 0 | 0 | 0 | 0.0 | 0.0 | 0 |

Table 6: unit element nodes with ± 0.1 nodal displacement

| Node | x | y | z | u_x | u_y | u_z |
|------|----|----|---|-------|-------|-------|
| 1 | -1 | -1 | 0 | -0.01 | -0.01 | 0 |
| 2 | 1 | -1 | 0 | 0.01 | -0.01 | 0 |
| 3 | 1 | 1 | 0 | 0.01 | 0.01 | 0 |
| 4 | -1 | 1 | 0 | -0.01 | 0.01 | 0 |
| 5 | 0 | -1 | 0 | 0.00 | -0.01 | 0 |
| 6 | 1 | 0 | 0 | 0.01 | 0.00 | 0 |
| 7 | 0 | 1 | 0 | 0.00 | 0.01 | 0 |
| 8 | -1 | 0 | 0 | -0.01 | 0.00 | 0 |
| 9 | 0 | 0 | 0 | 0.00 | 0.00 | 0 |

Table 7: unit element nodes with ± 0.01 nodal displacement

| Node | x | y | z | u_x | u_y | u_z |
|------|----|----|---|--------|--------|-------|
| 1 | -1 | -1 | 0 | -0.001 | -0.001 | 0 |
| 2 | 1 | -1 | 0 | 0.001 | -0.001 | 0 |
| 3 | 1 | 1 | 0 | 0.001 | 0.001 | 0 |
| 4 | -1 | 1 | 0 | -0.001 | 0.001 | 0 |
| 5 | 0 | -1 | 0 | 0.000 | -0.001 | 0 |
| 6 | 1 | 0 | 0 | 0.001 | 0.000 | 0 |
| 7 | 0 | 1 | 0 | 0.000 | 0.001 | 0 |
| 8 | -1 | 0 | 0 | -0.001 | 0.000 | 0 |
| 9 | 0 | 0 | 0 | 0.000 | 0.000 | 0 |

Table 8: unit element nodes with ± 0.001 nodal displacement

| Node | 1 | 2 | 3 | 4 | 5 | 6 | 7 | 8 | 9 |
|------|---------|---------|---------|---------|---------|---------|---------|---------|---------|
| 1 | 2.0078 | 0.1573 | -0.0786 | -0.2631 | -1.5683 | 0.2469 | 0.4504 | 0.0461 | -0.9985 |
| 2 | sym | 2.0078 | -0.2631 | -0.0786 | -1.5683 | 0.0461 | 0.4504 | 0.2469 | -0.9985 |
| 3 | sym | sym | 2.0078 | 0.1573 | 0.4504 | 0.0461 | -1.5683 | 0.2469 | -0.9985 |
| 4 | sym | sym | sym | 2.0078 | 0.4504 | 0.2469 | -1.5683 | 0.0461 | -0.9985 |
| 5 | -1.4055 | -1.4055 | sym | sym | 5.0359 | -1.1613 | -0.6294 | -1.1613 | -0.1736 |
| 6 | 0.2550 | 0.1356 | 0.1356 | 0.2550 | -0.9333 | 6.8918 | -0.9333 | 0.7922 | -6.5988 |
| 7 | sym | sym | -1.4055 | -1.4055 | sym | -1.1613 | 5.0359 | -1.1613 | -0.1736 |
| 8 | 0.1356 | 0.2550 | 0.2550 | 0.1356 | -0.9333 | sym | -0.9333 | 6.8918 | -6.5988 |
| 9 | -1.2589 | -1.2589 | -1.2589 | -1.2589 | -0.3038 | -5.9476 | -0.3038 | -5.9476 | 17.5389 |

Table 9: unit element stiffness coefficients k_{xx} for nodal coordinates and ± 0.1 displacements as in table (6), 3×3 Gausspoints, material stiffness parameters $\lambda = \mu = 1$ and element thickness $h_Z = 1$

| Node | 1 | 2 | 3 | 4 | 5 | 6 | 7 | 8 | 9 |
|------|---------|---------|---------|---------|---------|---------|---------|---------|---------|
| 1 | 1.3103 | 0.0641 | -0.0473 | -0.1954 | -0.9676 | 0.1634 | 0.3028 | 0.1058 | -0.7363 |
| 2 | sym | 1.3103 | -0.1954 | -0.0473 | -0.9676 | 0.1058 | 0.3028 | 0.1634 | -0.7363 |
| 3 | sym | sym | 1.3103 | 0.0641 | 0.3028 | 0.1058 | -0.9676 | 0.1634 | -0.7363 |
| 4 | sym | sym | sym | 1.3103 | 0.3028 | 0.1634 | -0.9676 | 0.1058 | -0.7363 |
| 5 | -0.9540 | -0.9540 | sym | sym | 3.5221 | -0.7499 | -0.3790 | -0.7499 | -0.3409 |
| 6 | 0.1641 | 0.1133 | 0.1133 | 0.1641 | -0.7309 | 4.6566 | -0.7309 | 0.3926 | -4.1424 |
| 7 | sym | sym | -0.9540 | -0.9540 | sym | -0.7499 | 3.5221 | -0.7499 | -0.3409 |
| 8 | 0.1133 | 0.1641 | 0.1641 | 0.1133 | -0.7309 | sym | -0.7309 | 4.6566 | -4.1424 |
| 9 | -0.7581 | -0.7581 | -0.7581 | -0.7581 | -0.3518 | -4.0880 | -0.3518 | -4.0880 | 11.9123 |

Table 10: unit element stiffness coefficients k_{xx} for nodal coordinates and ± 0.01 displacements as in table (7), 3×3 Gausspoints, material stiffness parameters $\lambda = \mu = 1$ and element thickness $h_Z = 1$

| Node | 1 | 2 | 3 | 4 | 5 | 6 | 7 | 8 | 9 |
|------|---------|---------|---------|---------|---------|---------|---------|---------|---------|
| 1 | 1.2509 | 0.0564 | -0.0447 | -0.1895 | -0.9166 | 0.1563 | 0.2902 | 0.1105 | -0.7136 |
| 2 | sym | 1.2509 | -0.1895 | -0.0447 | -0.9166 | 0.1105 | 0.2902 | 0.1563 | -0.7136 |
| 3 | sym | sym | 1.2509 | 0.0564 | 0.2902 | 0.1105 | -0.9166 | 0.1563 | -0.7136 |
| 4 | sym | sym | sym | 1.2509 | 0.2902 | 0.1563 | -0.9166 | 0.1105 | -0.7136 |
| 5 | -0.9153 | -0.9153 | sym | sym | 3.3920 | -0.7149 | -0.3578 | -0.7149 | -0.3541 |
| 6 | 0.1564 | 0.1113 | 0.1113 | 0.1564 | -0.7130 | 4.4653 | -0.7130 | 0.3592 | -3.9339 |
| 7 | sym | sym | -0.9153 | -0.9153 | sym | -0.7149 | 3.3920 | -0.7149 | -0.3541 |
| 8 | 0.1113 | 0.1564 | 0.1564 | 0.1113 | -0.7130 | sym | -0.7130 | 4.4653 | -3.9339 |
| 9 | -0.7157 | -0.7157 | -0.7157 | -0.7157 | -0.3551 | -3.9285 | -0.3551 | -3.9285 | 11.4304 |

Table 11: unit element stiffness coefficients k_{xx} for nodal coordinates and ± 0.001 displacements as in table (8), 3×3 Gausspoints, material stiffness parameters $\lambda = \mu = 1$ and element thickness $h_Z = 1$

| Node | x | y | z | F_x | F_y | F_z | Equilibrium Iteration | $u_x^{N1,N2,N3,N4}$ $u_y^{N1,N2,N3,N4}$ | $u_x^{N5,N6,N7,N8}$ $u_y^{N5,N6,N7,N8}$ | $u_z^{N1,N2,N3,N4}$ $u_z^{N5,N6,N7,N8}$ |
|------|----|----|---|--------|--------|--------|-----------------------|--------------------------------------------|--------------------------------------------|--------------------------------------------|
| 1 | -1 | -1 | 0 | -0.01 | -0.01 | 0 | 1 | ± 0.006250 | 0 | 0 |
| 2 | 1 | -1 | 0 | 0.01 | -0.01 | 0 | 2 | ± 0.005874 | 0 | 0 |
| 3 | 1 | 1 | 0 | 0.01 | 0.01 | 0 | 3 | ± 0.005918 | 0 | 0 |
| 4 | -1 | 1 | 0 | -0.01 | 0.01 | 0 | 4 | ± 0.005913 | 0 | 0 |
| 5 | 0 | -1 | 0 | \div | \div | \div | 5 | ± 0.005914 | 0 | 0 |
| 6 | 1 | 0 | 0 | \div | \div | \div | | | | |
| 7 | 0 | 1 | 0 | \div | \div | \div | | | | |
| 8 | -1 | 0 | 0 | \div | \div | \div | | | | |
| 9 | 0 | 0 | 0 | \div | \div | \div | | | | |

Table 12: unit element corner force exposed, 3×3 Gausspoints, material stiffness parameters $\lambda = \mu = 1$ and element thickness $h_Z = 1$ with iterationwise displacement solution for corner nodes 1, 2, 3 and 4

| Node | x | y | z | F_x | F_y | F_z | Equilibrium Iteration | $u_x^{N1,N2,N3,N4}$ $u_y^{N1,N2,N3,N4}$ | $u_x^{N5,N6,N7,N8}$ $u_y^{N5,N6,N7,N8}$ | $u_z^{N1,N2,N3,N4}$ $u_z^{N5,N6,N7,N8}$ |
|------|----|----|---|--------|--------|--------|-----------------------|--------------------------------------------|--------------------------------------------|--------------------------------------------|
| 1 | -1 | -1 | 0 | -0.01 | -0.01 | 0 | 1 | ± 0.006634 | ± 0.002307 | 0 |
| 2 | 1 | -1 | 0 | 0.01 | -0.01 | 0 | 2 | ± 0.006314 | ± 0.002271 | 0 |
| 3 | 1 | 1 | 0 | 0.01 | 0.01 | 0 | 3 | ± 0.006330 | ± 0.002272 | 0 |
| 4 | -1 | 1 | 0 | -0.01 | 0.01 | 0 | 4 | ± 0.006330 | ± 0.002272 | 0 |
| 5 | 0 | -1 | 0 | 0.00 | -0.01 | 0 | | | | |
| 6 | 1 | 0 | 0 | 0.01 | 0.00 | 0 | | | | |
| 7 | 0 | 1 | 0 | 0.00 | 0.01 | 0 | | | | |
| 8 | -1 | 0 | 0 | -0.01 | 0.00 | 0 | | | | |
| 9 | 0 | 0 | 0 | \div | \div | \div | | | | |

Table 13: unit element corner and edge midpoint force exposed, 3×3 Gausspoints, material stiffness parameters $\lambda = \mu = 1$ and element thickness $h_Z = 1$ with iterationwise displacement solution for corner nodes 1, 2, 3 and 4 and edge midpoint nodes 5, 6, 7 and 8

| Node | x | y | z | F_x | F_y | F_z | Equilibrium Iteration | $u_x^{N1,N2,N3,N4}$ $u_y^{N1,N2,N3,N4}$ | $u_x^{N5,N6,N7,N8}$ $u_y^{N5,N6,N7,N8}$ | $u_z^{N1,N2,N3,N4}$ $u_z^{N5,N6,N7,N8}$ |
|------|----|----|---|--------|--------|--------|-----------------------|--------------------------------------------|--------------------------------------------|--------------------------------------------|
| 1 | -1 | -1 | 0 | -0.01 | -0.01 | 0 | 1 | ± 0.066346 | ± 0.023076 | 0 |
| 2 | 1 | -1 | 0 | 0.01 | -0.01 | 0 | 2 | ± 0.041951 | ± 0.019947 | 0 |
| 3 | 1 | 1 | 0 | 0.01 | 0.01 | 0 | 3 | ± 0.050051 | ± 0.020686 | 0 |
| 4 | -1 | 1 | 0 | -0.01 | 0.01 | 0 | 4 | ± 0.047099 | ± 0.020445 | 0 |
| 5 | 0 | -1 | 0 | 0.00 | -0.01 | 0 | 5 | ± 0.048151 | ± 0.020529 | 0 |
| 6 | 1 | 0 | 0 | 0.01 | 0.00 | 0 | 10 | ± 0.047873 | ± 0.020507 | 0 |
| 7 | 0 | 1 | 0 | 0.00 | 0.01 | 0 | 25 | ± 0.047872 | ± 0.020507 | 0 |
| 8 | -1 | 0 | 0 | -0.01 | 0.00 | 0 | 26 | ± 0.047872 | ± 0.020507 | 0 |
| 9 | 0 | 0 | 0 | \div | \div | \div | | | | |

Table 14: unit element corner and edge midpoint force exposed, 3×3 Gausspoints, material stiffness parameters $\lambda = \mu = 1$ and element thickness $h_Z = 0.1$ with iterationwise displacement solution for corner nodes 1, 2, 3 and 4 and edge midpoint nodes 5, 6, 7 and 8

| Node | x | y | z | F_x | F_y | F_z | Equilibrium Iteration | $u_x^{N5,N6,N7,N8}$ $u_y^{N5,N6,N7,N8}$ | $u_z^{N5,N6,N7,N8}$ | u_z^{N9} |
|------|----|----|---------|--------|--------|-----------|-----------------------|--------------------------------------------|---------------------|-------------|
| 1 | -1 | -1 | 0 | \div | \div | \div | | | | |
| 2 | 1 | -1 | 0 | \div | \div | \div | | | | |
| 3 | 1 | 1 | 0 | \div | \div | \div | | | | |
| 4 | -1 | 1 | 0 | \div | \div | \div | | | | |
| 5 | 0 | -1 | 0 | 0 | 0 | 0 | | | | |
| 6 | 1 | 0 | 0 | 0 | 0 | 0 | | | | |
| 7 | 0 | 1 | 0 | 0 | 0 | 0 | | | | |
| 8 | -1 | 0 | 0 | 0 | 0 | 0 | | | | |
| 9 | 0 | 0 | 0.01000 | 0 | 0 | 10^{-5} | Case 1: 100 | ± 0.000752 | 0.015282 | 0.020794 |
| 9 | 0 | 0 | 0.00100 | 0 | 0 | 10^{-5} | Case 2: 100 | ± 0.011081551 | 0.062530450 | 0.105609499 |
| 9 | 0 | 0 | 0.00010 | 0 | 0 | 10^{-5} | Case 3: 100 | ± 0.011094136 | 0.062621772 | 0.106090596 |
| 9 | 0 | 0 | 0.00001 | 0 | 0 | 10^{-5} | Case 4: 100 | ± 0.011095423 | 0.062630868 | 0.106138805 |

Table 15: unit element out-of-plane center force exposed, 3×3 Gausspoints, material stiffness parameters $\lambda = \mu = 10^{10}$ and element thickness $h_z = 0.001$ with converged displacement solution for edge midpoint nodes 5, 6, 7 and 8 and central node 9 for different cases of out-of-plane initial position of central node 9

| Node | x | y | z | u_x Cases 1, 2, 3 | u_y Cases 1, 2, 3 | u_z Case 1 | u_z Case 2 | u_z Case 3 |
|------|--------|--------|----------|------------------------|------------------------|-----------------|-----------------|-----------------|
| 1 | -1 | -1 | 0 | 0 | 0 | 0 | 0 | 0 |
| 2 | 1 | -1 | 0 | 0 | 0 | 0 | 0 | 0 |
| 3 | 1 | 1 | 0 | 0 | 0 | 0 | 0 | 0 |
| 4 | -1 | 1 | 0 | 0 | 0 | 0 | 0 | 0 |
| 5 | 0 | -1 | 0 | 0 | 0 | 0 | 0 | 0 |
| 6 | 1 | 0 | 0 | 0 | 0 | 0 | 0 | 0 |
| 7 | 0 | 1 | 0 | 0 | 0 | 0 | 0 | 0 |
| 8 | -1 | 0 | 0 | 0 | 0 | 0 | 0 | 0 |
| 9 | 0.000 | 0.000 | 0.001000 | 0.00000 | 0.00000 | 0.00324 | 0.00303 | 0.00296 |
| 18 | 0.000 | -0.500 | 0.000750 | 0.00000 | 0.00000 | \div | 0.00181 | 0.00171 |
| 22 | -0.500 | -0.500 | 0.000563 | 0.00000 | 0.00000 | \div | 0.00155 | 0.00148 |
| 289 | -0.125 | 0.125 | 0.000969 | 0.00000 | 0.00000 | \div | \div | 0.00278 |

Table 16: unit membrane out-of-plane eigenload exposed, 3×3 Gausspoints per element, material stiffness parameters $\lambda = \mu = 10^{10}$, material density $\rho = 1000$, membrane thickness $h_z = 0.001$ and gravity $g_z = 10$ with converged displacement solutions for different nodes on the inner of the unit membrane for discretization with one element (case 1), with 2×2 elements (case 2) and with 8×8 elements (case 3)

5.1 Out-of-plane work load on Hypar shaped membrane

A Hypar shaped membrane with quadratic ground-section and edge length of 5 m is exposed to out-of-plane work load. Corner out-of-plane z-coordinates of the Hypar shaped membrane are ± 0.0625 m. Material stiffness parameters are $\lambda = 10^{10}$ N/m² and $\mu = 10^{10}$ N/m² (equivalent to modulus of elasticity $E = 2.5 \cdot 10^{10}$ N/m² and Poisson ratio $\nu = 0.25$), material density is $\rho = 1000$ kg/m³, membrane thickness is $h_z = 0.001$ m, gravity is $g_z = 10$ m/s². The membrane is exposed to a distributed load of 1000 N/m² (100 times its eigenload, e.g. due to snow) in out-of-plane z-direction. The membrane is meshed with 8×8 quadratic 9-node-4-corner elements (289 nodes). Cartesian coordinates of the undeformed initial stress free membrane shape for corner nodes, edge midpoint nodes, central node and several other nodes on the inner of the membrane are shown in table (17) together with the converged displacement solution for these selected nodes. Central node 9 out-of-plane z-displacement is largest with 0.00906... m, followed by surrounding nodes 287 and 289 with z-displacement of 0.00502... m and nodes 286 and 288 with z-displacement of 0.00444... m. Further outward positioned nodes 18, 20, 19 and 21 (z-displacement all 0.000056... m) on the main axes as well as nodes 22, 24 (z-displacement both 0.0000002... m), 23 and 25 (z-displacement both 0.0000004... m) on the diagonal axes show much smaller out-of-plane z-displacement. This indicates that out-of-plane z-displacement appears to the largest amount in the center of the membrane and its vicinity where the slope of the membrane with respect to out-of-plane z-direction is minimum and therefore the membrane has least stiffness with respect to out-of-plane z-direction. The converged displacement solution for the considered Hypar shaped membrane shows full symmetry.

Altogether an out-of-plane z-displacement of 0.00906... m in the center of the membrane induced by an out-of-plane load in z-direction of 1000 N/m² (e.g. due to snow) with a membrane thickness of $h_z = 0.001$ m, an edge length of 5 m and corner out-of-plane z-coordinates of ± 0.0625 m appears acceptable. Initial undeformed stress free shape of the Hypar shaped membrane and out-of-plane z-displacement distribution due to out-of-plane load in z-direction of 1000 N/m² (e.g. due to snow) are shown in figure 3. It becomes obvious that out-of-plane z-displacement is approximately zero although the membrane except for the center and its vicinity where out-of-plane z-displacement is remarkable compared with all other regions of the membrane. This demonstrated the shape-inherent stiffness of the Hypar shape itself (except for the center and its vicinity). For to visualize the shape of the Hypar shaped membrane and its remarkable out-of-plane z-displacement in the center and its vicinity the out-of-plane z-coordinate of the initial undeformed stress free shape and the out-of-plane z-displacement are also plotted with scale-enlargened factor 10 in figure 3.

5.2 Horizontal pressure load on 3D spinnaker sail membrane

A 3D spinnaker sail membrane is exposed to horizontal external load that represents air flow pressure onto the sail membrane. The sail membrane has a total height of 40 m on its vertical center line and a total width of 20 m along its curved bottom. The shape of the sail membrane is characterized by a maximum out-of-plane y-coordinate of 5 m at 18.5 m vertical distance measured from its bottom line midpoint. The sail is completely fixed

in displacement for all three cartesian directions at its' four corners. The sail membrane is fixed in out-of-plane y-direction along its outer boundary on its curved bottom line, on both curved side lines and on the short top line of length 2 m (which altogether models a trapezoidal boundary of the curved-in-3D-space sail membrane that approximates a curved-in-3D-space triangular shape). Material stiffness parameters are $\lambda=10^{10}$ N/m² and $\mu=10^{10}$ N/m² (equivalent to modulus of elasticity $E=2.5 \cdot 10^{10}$ N/m² and Poisson ratio $\nu=0.25$), material density is $\rho=1000$ kg/m³, membrane thickness is $h_z=0.001$ m. The membrane is meshed with 8×8 quadratic 9-node-4-corner elements (289 nodes). Cartesian coordinates of the undeformed initial stress free membrane shape for corner nodes, edge midpoint nodes, the central node and other nodes on the inner of the membrane are shown in table (18). The sail membrane is exposed to horizontal out-of-plane load in y-direction of amount 10 N/m² (case 1, air flow pressure $p_1=0.5\rho_{air}v_{air,1}^2$, $\rho_{air}=1.25$ kg/m³, $v_{air,1}=4$ m/s) and of amount 100 N/m² (case 2, air flow pressure $p_2=0.5\rho_{air}v_{air,2}^2$, $v_{air,2}=12.65$ m/s).

Displacement for selected nodes on the membrane for cases 1 and 2 is shown in table (18). Cartesian components of displacement distribution as well as the magnitude of displacement distribution over the spinnaker sail membrane for cases 1 and 2 are illustrated in figure 4. The displacement solution for both cases 1 and 2 shows approximate symmetry with regard to the vertical center line. Displacement for case 2 ($v_{air,2}=12.65$ m/s) appears altogether larger than for case 1 ($v_{air,1}=4$ m/s). Largest displacement for both cases 1 and 2 appears in the lower third of the spinnaker sail membrane, where largest amount of displacement takes place in out-of-plane y-direction. In the lower third of the membrane on lateral side range transversal horizontal x-displacement is directed outward. The top range of the membrane in the upper third of the membrane is z-displaced vertically upward whereas in its lower third the membrane is z-displaced vertically downward. A distinction between case 1 and case 2 can be made regarding the out-of-plane y-displacement in the lower third of the membrane: For case 1 the respective out-of-plane y-displacement appears around the vertical center line and is of approximately 0.035 m ($v_{air,1}=4$ m/s). For case 2, in contrast, the respective out-of-plane y-displacement appears symmetrically on the lateral side range and is approximately 0.086 m ($v_{air,2}=12.65$ m/s). That means that for case 2 the spinnaker sail membrane is flattened in its lower third to an obviously higher degree than it is for case 1. Opposite to the lower third of the membrane for comparison between case 1 and case 2, in the upper third of the membrane for comparison between case 1 and case 2 it shows that for case 1 the lateral range is out-of-plane y-displaced the most whereas for case 2 maximum out-of-plane y-displacement in the upper third of the membrane appears on the vertical center line of the membrane, i.e. in the upper third of the membrane for case 1 the spinnaker sail membrane is flattened whereas it is funnel-shaped sharpened in the upper third of the membrane for case 2.

6 Conclusion

The governing equation for 3D membrane structures with tangential tensile stresses only is expressed by a virtual work approach. Parametric description of the undeformed initial stress free shape of the membrane and its 3D cartesian displacement is applied. Constitutive relation between structural membrane stress and structural membrane strain is

| Node | x [m] | y [m] | z [m] | u_x [m] | u_y [m] | u_z [m] |
|------|---------|---------|---------------|-----------|-----------|--------------|
| 1 | -2.5 | -2.5 | -0.0625000000 | 0 | 0 | 0 |
| 2 | 2.5 | -2.5 | 0.0625000000 | 0 | 0 | 0 |
| 3 | 2.5 | 2.5 | -0.0625000000 | 0 | 0 | 0 |
| 4 | -2.5 | 2.5 | 0.0625000000 | 0 | 0 | 0 |
| 5 | 0 | -2.5 | 0 | 0 | 0 | 0 |
| 6 | 2.5 | 0 | 0 | 0 | 0 | 0 |
| 7 | 0 | 2.5 | 0 | 0 | 0 | 0 |
| 8 | -2.5 | 0 | 0 | 0 | 0 | 0 |
| 9 | 0 | 0 | 0 | 0 | 0 | 0.0090626542 |
| 286 | -0.3125 | -0.3125 | -0.0009765625 | 0 | 0 | 0.0044405393 |
| 287 | 0.3125 | -0.3125 | 0.0009765625 | 0 | 0 | 0.0050201298 |
| 288 | 0.3125 | 0.3125 | -0.0009765625 | 0 | 0 | 0.0044405393 |
| 289 | -0.3125 | 0.3125 | 0.0009765625 | 0 | 0 | 0.0050201298 |
| 18 | 0 | -1.2500 | 0 | 0 | 0 | 0.0000562882 |
| 19 | 1.2500 | 0 | 0 | 0 | 0 | 0.0000562882 |
| 20 | 0 | 1.2500 | 0 | 0 | 0 | 0.0000562882 |
| 21 | -1.2500 | 0 | 0 | 0 | 0 | 0.0000562882 |
| 22 | -1.2500 | -1.2500 | -0.0156250000 | 0 | 0 | 0.0000004338 |
| 23 | 1.2500 | -1.2500 | 0.0156250000 | 0 | 0 | 0.0000002372 |
| 24 | 1.2500 | 1.2500 | -0.0156250000 | 0 | 0 | 0.0000004338 |
| 25 | -1.2500 | 1.2500 | 0.0156250000 | 0 | 0 | 0.0000002372 |

Table 17: Hypar shaped membrane exposed to 1000 N/m^2 (100 times its out-of-plane eigenload), 3×3 Gausspoints per element, material stiffness parameters $\lambda = \mu = 10^{10} \text{ N/m}^2$, material density $\rho = 1000 \text{ kg/m}^3$, membrane thickness $h_Z = 0.001 \text{ m}$ and gravity $g_Z = 10 \text{ m/s}^2$ with converged displacement solution for different nodes on the inner of the membrane for discretization with 8×8 elements

| Node | x [m] | y [m] | z [m] | u_x [m] Case 1 | u_y [m] Case 1 | u_z [m] Case 1 | u_x [m] Case 2 | u_y [m] Case 2 | u_z [m] Case 2 |
|------|---------|---------|--------|---------------------|---------------------|---------------------|---------------------|---------------------|---------------------|
| 1 | -10 | 0 | 0 | 0 | 0 | 0 | 0 | 0 | 0 |
| 2 | 10 | 0 | 0 | 0 | 0 | 0 | 0 | 0 | 0 |
| 3 | 1 | 40 | 0 | 0 | 0 | 0 | 0 | 0 | 0 |
| 4 | -1 | 40 | 0 | 0 | 0 | 0 | 0 | 0 | 0 |
| 5 | 0 | 3 | 0 | -0.00001 | 0.00071 | 0 | 0.00007 | 0.00207 | 0 |
| 6 | 3.6363 | 20 | 0 | 0.00132 | 0.00023 | 0 | 0.00659 | 0.00207 | 0 |
| 7 | 0 | 40 | 0 | -0.00010 | -0.00011 | 0 | 0.00272 | -0.00077 | 0 |
| 8 | -3.6363 | 20 | 0 | -0.00143 | 0.00025 | 0 | -0.00751 | 0.00222 | 0 |
| 9 | 0 | 21.5 | 5 | -0.00008 | 0.00000 | 0.00319 | 0.00009 | 0.00122 | 0.00567 |
| 286 | -0.5059 | 19.1611 | 4.8273 | -0.00446 | -0.00094 | 0.01454 | -0.00459 | 0.00038 | 0.01390 |
| 287 | 0.5059 | 19.1611 | 4.8273 | 0.00430 | -0.00094 | 0.01452 | 0.00492 | 0.00034 | 0.01456 |
| 288 | 0.4063 | 23.7920 | 4.8273 | 0.00243 | 0.00053 | 0.00650 | 0.00619 | 0.00229 | 0.01392 |
| 289 | -0.4063 | 23.7920 | 4.8273 | -0.00270 | 0.00053 | 0.00645 | -0.00609 | 0.00231 | 0.01428 |
| 18 | 0 | 12.2500 | 3.5355 | -0.00006 | -0.00992 | 0.03400 | 0.00004 | 0.00017 | 0.00515 |
| 19 | 1.8180 | 21.1250 | 3.7500 | 0.00371 | 0.00033 | 0.00216 | 0.00420 | 0.00159 | 0.00059 |
| 20 | 0 | 30.7500 | 3.5355 | -0.00007 | -0.00228 | -0.00737 | 0.00110 | 0.01618 | 0.05217 |
| 21 | -1.8180 | 21.1250 | 3.7500 | -0.00359 | 0.00032 | 0.00194 | -0.00634 | 0.00177 | 0.00235 |
| 22 | -2.7500 | 11.6875 | 2.6517 | -0.02213 | -0.00525 | 0.03731 | -0.04541 | -0.01177 | 0.08425 |
| 23 | 2.7500 | 11.6875 | 2.6517 | 0.02191 | 0.00522 | 0.03691 | 0.04917 | -0.01269 | 0.08837 |
| 24 | 1.1029 | 30.5625 | 2.6517 | 0.00511 | 0.00090 | 0.00298 | 0.00718 | 0.00138 | 0.00472 |
| 25 | -1.1029 | 30.5625 | 2.6517 | -0.00448 | 0.00075 | 0.00244 | -0.01029 | 0.00201 | 0.00704 |

Table 18: 3D spinnaker sail membrane exposed to out-of-plane horizontal load of 10 N/m^2 (case 1) and of 100 N/m^2 (case 2), corner nodes, edge midpoint nodes, central node and other node on the inner of the membrane, 3×3 Gausspoints per element, material stiffness parameters $\lambda = \mu = 10^{10} \text{ N/m}^2$ and membrane thickness $h_z = 0.001 \text{ m}$ with out-of-plane initial position of central node 9

assumed linear. The governing equation can refer either to the undeformed state of the membrane structure with 2nd Piola-Kirchhoff stress and Green-Lagrange strain or to the deformed state of the membrane structure with Cauchy stress and Euler-Almansi strain. Consideration of full nonlinearity of membrane stress and linearized virtual membrane strain leads to a fully consistent description of the stated problem. Spatial discretization is performed by introduction of 9-node-4-corner finite elements with quadratic polynomials for interpolation of displacement within each element. Time discretization is performed by the HHT- α method. The resulting discrete nonlinear equation system is solved in an iterative manner for the unknown displacement of the considered membrane structure. Evaluation of the numeric approach on the unit 9-node-4-corner element is performed in detail: Interpolation of displacement within the element is checked. The nonlinearly (super-linearly) increasing in-plane stiffness of the membrane for linearly increasing in-plane displacement is demonstrated; appropriate stiffness matrix coefficients for in-plane displacement are shown. Zero out-of-plane stiffness for completely even membranes is demonstrated. Mass matrix coefficients for the unit membrane element are shown. In-plane displacement due to in-plane external forces is determined in dependence on boundary conditions for corner nodes and edge midpoint nodes. Geometric out-of-plane stiffness due to out-of-plane external forces is evaluated and assessed in dependence on the out-of-plane shape of the membrane and in dependence on the discretization level (number of elements in the finite element mesh). For symmetric out-of-plane load (eigenload) the stress distribution within the unit membrane shows complete symmetry where in the outer part of the membrane tensile stresses appear whereas in the center of the membrane (for a parabolic out-of-plane shape of the undeformed stress free membrane) the state of force equilibrium is indifferent (i.e. the displacement field in the vicinity of the membrane center indicates that compression of the membrane occurs and thus no tensile stresses act in and around the membrane center).

Application of the numeric approach to a Hypar shaped membrane with square ground-section that is exposed to 100 times its out-of-plane eigenload (e.g. due to snow) demonstrates the high stiffness of the Hypar shape against out-of-plane load with small out-of-plane displacement except for the center of the membrane where the slope of the membrane with respect to out-of-plane direction is least within the membrane and therefore the membrane center experiences largest out-of-plane displacement. Application of the numeric approach to a spinnaker sail membrane that is exposed to horizontal pressure load that represents air flow shows characteristic deformation of the sail. Deformation patterns due to two different air flow velocities are compared with each other.

REFERENCES

- [1] O. Frei. *Das haengende Dach*. Technische Universitaet Berlin, 1954
- [2] K.-U. Bletzinger. Formfindung von leichten Tragwerken. in *Baustatik-Baupraxis* (Hrsg. D. Dinkler), 99-110, Institut fuer Statik, Technische Universitaet Braunschweig, 2002
- [3] K.-J. Bathe. *Finite-Elemente-Methoden*. Springer-Verlag Berlin, 2002

- [4] H. M. Hilber, T. J. R. Hughes, R. L. Taylor. Improved numerical dissipation for time integration algorithms in structural dynamics. *Earthquake engineering and structural dynamics*, vol. 5, 283-292, 1977
- [5] O. Frei et al. Mitteilungen der Entwicklungsstelle fuer den Leichtbau in Berlin. Nr. 7, Nr. 8, Nr. 9. Entwicklungsstelle fuer den Leichtbau in Berlin, 1961-1963
- [6] O. Frei, R. Trostel. *Zugbeanspruchte Konstruktionen*, Band 1. Ullstein Fachverlag Berlin/Frankfurt, 1962
- [7] O. Frei, F.-K. Schleyer. *Zugbeanspruchte Konstruktionen*, Band 2. Ullstein Fachverlag Berlin/Frankfurt, 1966
- [8] C. Roland. *Frei Otto – Spannweiten*. Ullstein Fachverlag Berlin/Frankfurt, 1965
- [9] *Weitgespannte Flaechentragwerke*, Band 1 bis 3. Internationales Symposium Weitgespannte Flaechentragwerke, SFB 64, Universitaet Stuttgart, 1976
- [10] H. Dirlwanger et al. *Ausgewahlte Flaechentragwerke*. Internationales Symposium Weitgespannte Flaechentragwerke, SFB 64, Universitaet Stuttgart, 1976
- [11] J. Zerning. Design guide to anticlastic structures in plastic. Polytec of London, 1975
- [12] E. Bubner et al. *Minimalstrukturen*. Symposium Universitaet Essen Gesamthochschule, 1977
- [13] *Weitgespannte Flaechentragwerke*. Band 1 und 2. Internationales Symposium Weitgespannte Flaechentragwerke, SFB 64, Universitaet Stuttgart, 1979
- [14] E. Bubner et al. *Membrankonstruktionen*, Teil 1, Teil 2, Teil 3, Teil 4. Haus der Technik Essen / Universitaet Essen Gesamthochschule, 1979-1982
- [15] G. Brinkmann (Hrsg.). *Weitgespannte Flaechentragwerke*. Zusammenfassender Bericht, SFB 64, Universitaet Stuttgart, 1990
- [16] P. Drew. *Tensile structures*. Granada publishing London, 1979
- [17] H. Berger. *Light structures – structures of light*. Birkhaeuser, Basel/Boston/Berlin, 1996
- [18] H.-J. Schock. *Segel, Folien und Membranen*. Birkhaeuser, Basel/Boston/Berlin, 1997
- [19] D. Hoppe. textile Membrankonstruktionen. Boehlau Verlag Wien/Koeln/Weimar, 2007
- [20] P. Drew. *New tent architecture*. Thames and Hudson, 2007
- [21] W. Renner. Membrantragwerke – Konzepte, Bemessung, Ausfuehrung. *Stahlbau* 69, Heft 7, 2000
- [22] H. Apelmann, C. Gengnagel. Interaktion von Membranen und biegesteifen Bogen-tragwerken. *Stahlbau* 72, Heft 10, 702-707, 2003
- [23] K. Goeppert. Membrankonstruktionen – Form und Detail. *Stahlbau* 73, Heft 12, 990-1000, 2004
- [24] J. Cremers, G. Grunwald. Innovative Membran-Stadiondaecher in Kiew, Warschau und Vancouver. *Stahlbau* 80, Heft 9, 678-686, 2011

- [25] M. Seel, G. Siebert. Analytische Loesungen fuer Kreis- und Kreisringplatten unter symmetrischer und antimetrischer Einwirkung. Stahlbau 81, Heft 9, 711-718, 2012
- [26] S. Neuhaeuser et al. Adaptive Tragwerke – Aktuelle Forschung im Ultraleichtbau. Stahlbau 82, Heft 6, 428-437, 2013
- [27] K. Linkwitz, H.-J. Schek. Einige Bemerkungen zur Berechnung von vorgespannten Seilnetzkonstruktionen. Ingenieur-Archiv 40, 145-158, 1971
- [28] H. Buefler. Pressure loaded structures under large deformations. Zeitschrift fuer Angewandte Mathematik und Mechanik 64, Heft 7, 287-295, 1984
- [29] K.-U. Bletzinger, E. Ramm. Structural optimization and form finding of light weight structures. Computers and Structures 79, 2053-2962, 2001
- [30] R. Wuechner, K.-U. Bletzinger. Stress-adapted numerical form finding of pre-stressed surfaces by updated reference strategy. International Journal for Numerical Methods in Engineering 64, 143-166, 2005
- [31] R. Wuechner. Mechanik und Numerik der Formfindung und Fluid-Struktur-Interaktion von Membrantragwerken. TU Muenchen, 2006
- [32] J. Linhard. Numerisch-mechanische Betrachtung des Entwurfsprozesses von Membrantragwerken. TU Muenchen, 2009
- [33] C. Corte, J. Garcia, E. Onate. Three-dimensional flow around rigid and elastic cylindrical structures. CIMNE Barcelona, 2007
- [34] C. Corte, J. Garcia, E. Onate. A strongly-coupled segregated approach for finite element modeling of fluid-structure interaction. CIMNE Barcelona, 2008
- [35] C. Corte. A segregated approach for strong coupling of finite element solvers to model fluid-structure interaction. CIMNE Barcelona, 2008
- [36] C. Corte. A 3D approach for finite element modeling of viscous fluid flow. Dr. C. Corte, Baustatik – Baudynamik – Numerische Modellierung, Berlin, Tel./Fax +49-(0)30-347871 78/80, 2010
- [37] C. Corte. A 3D approach for finite element modeling of fluid-structure interaction between incompressible viscous fluids and elastic structures. Dr. C. Corte, Baustatik – Baudynamik – Numerische Modellierung, Berlin, Tel./Fax +49-(0)30-347871 78/80, 2011
- [38] C. Corte. Finite element modeling of fluid-structure interaction for an elastic 2D flag in harmonic viscous fluid flow and an elastic 3D sail structure in stationary viscous fluid flow. Dr. C. Corte, Baustatik – Baudynamik – Numerische Modellierung, Berlin, Tel./Fax +49-(0)30-347871 78/80, 2012

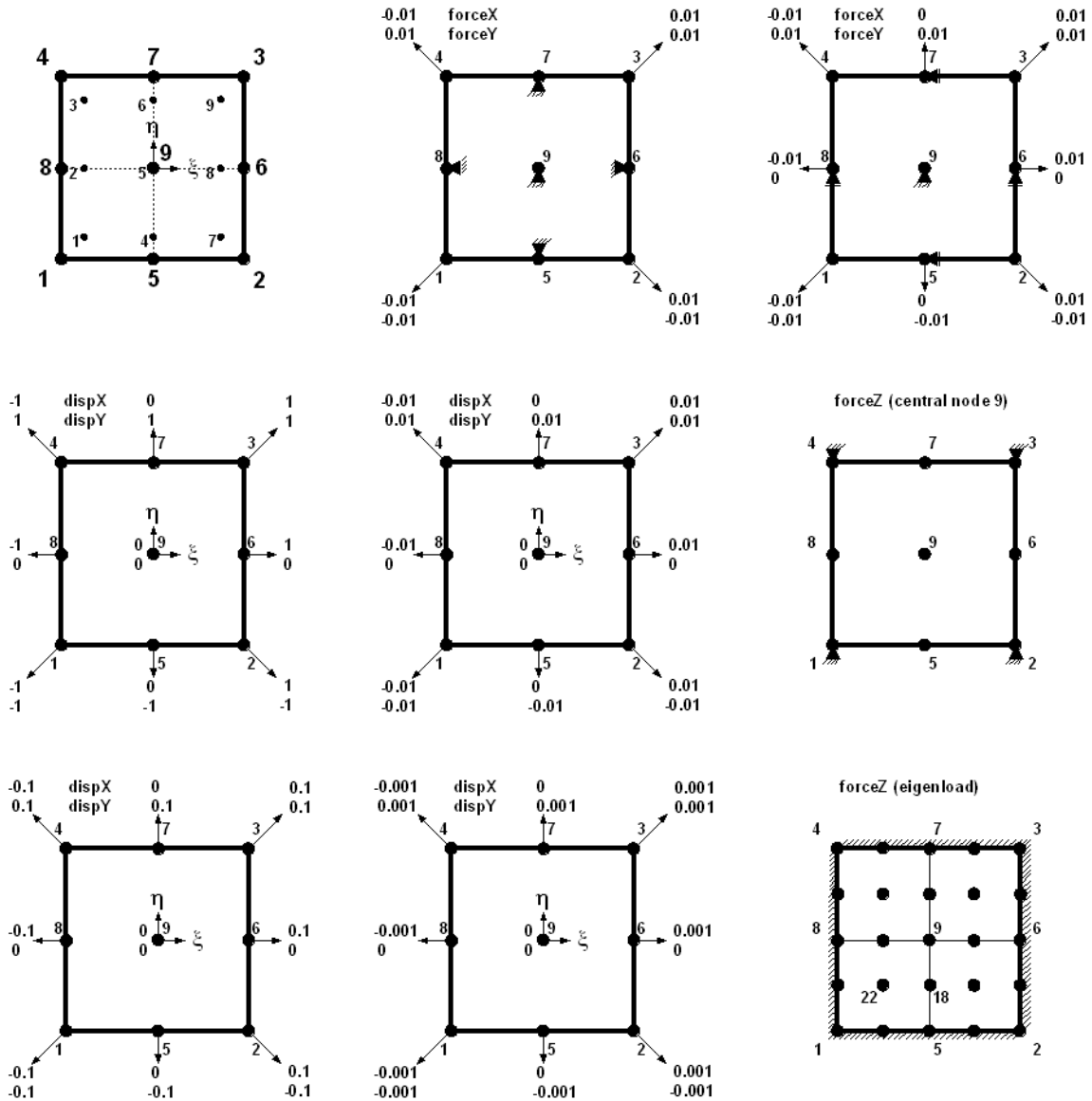


Figure 1: membrane evaluation: 4.1 (top left): 9-node-4-corner membrane unit element with node numbers (outer) and Gauss point numbers (inner); 4.2 (center left): corner and edge midpoint displacement ± 1 on unit element; 4.3 (bottom left): corner and edge midpoint displacement ± 0.1 on unit element; 4.3 (center): corner and edge midpoint displacement ± 0.01 on unit element; 4.3 (bottom center): corner and edge midpoint displacement ± 0.001 on unit element; 4.4 (top center): in-plane corner x- and y-force ± 0.01 on unit element, fixed edge midpoints, fixed center; 4.5 (top right): in-plane corner and edge midpoint x- and y-force ± 0.01 on unit element, tangentially fixed edge midpoints, fixed center; 4.6 (center right): out-of-plane center z-force $+10^{-5}$ on unit element, fixed corners; 4.7 (bottom right): out-of-plane eigenload on unit element, fixed boundary

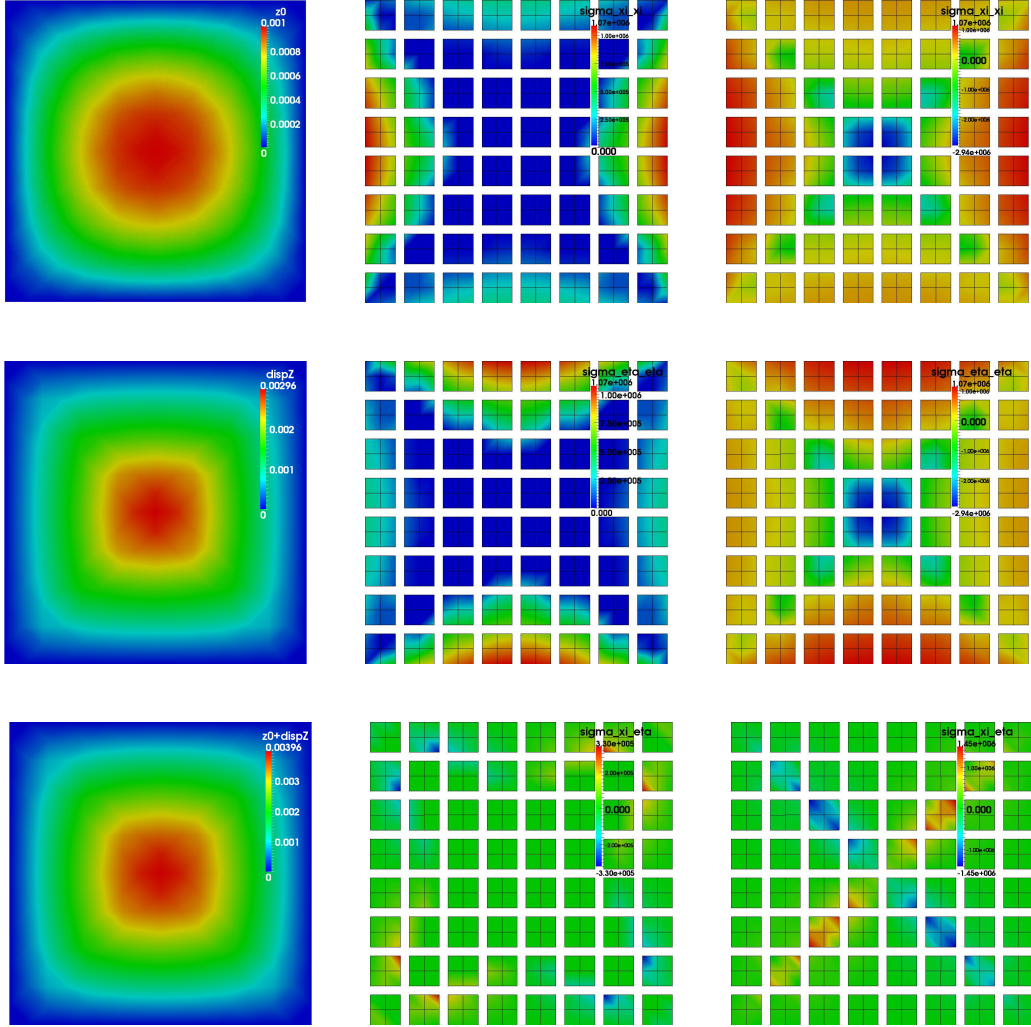


Figure 2: membrane evaluation 4.7: membrane with initial undeformed stress free out-of-plane shape $z(x,y)=0.001 \cdot (x-1)(x+1)(y-1)(y+1)$ exposed to out-of-plane eigenload for 8×8 elements: left column: out-of-plane initial shape z-coordinate; out-of-plane z-displacement; sum of out-of-plane initial shape z-coordinate and out-of-plane z-displacement; center column: membrane stress $S_{\xi\xi}(\xi, \eta)$ on Gausspoints (3×3 Gausspoints per element) for tensile stiffness only; membrane stress $S_{\eta\eta}(\xi, \eta)$ on Gausspoints (3×3 Gausspoints per element) for tensile stiffness only; membrane stress $S_{\xi\eta}(\xi, \eta)$ on Gausspoints (3×3 Gausspoints per element) for tensile stiffness only; right column: membrane pseudo stress $S_{\xi\xi}^{pseudo}(\xi, \eta)$ on Gausspoints (3×3 Gausspoints per element) for tensile stiffness and pseudo-compressive stiffness; membrane pseudo stress $S_{\eta\eta}^{pseudo}(\xi, \eta)$ on Gausspoints (3×3 Gausspoints per element) for tensile stiffness and pseudo-compressive stiffness; membrane pseudo stress $S_{\xi\eta}^{pseudo}(\xi, \eta)$ on Gausspoints (3×3 Gausspoints per element) for tensile stiffness and pseudo-compressive stiffness

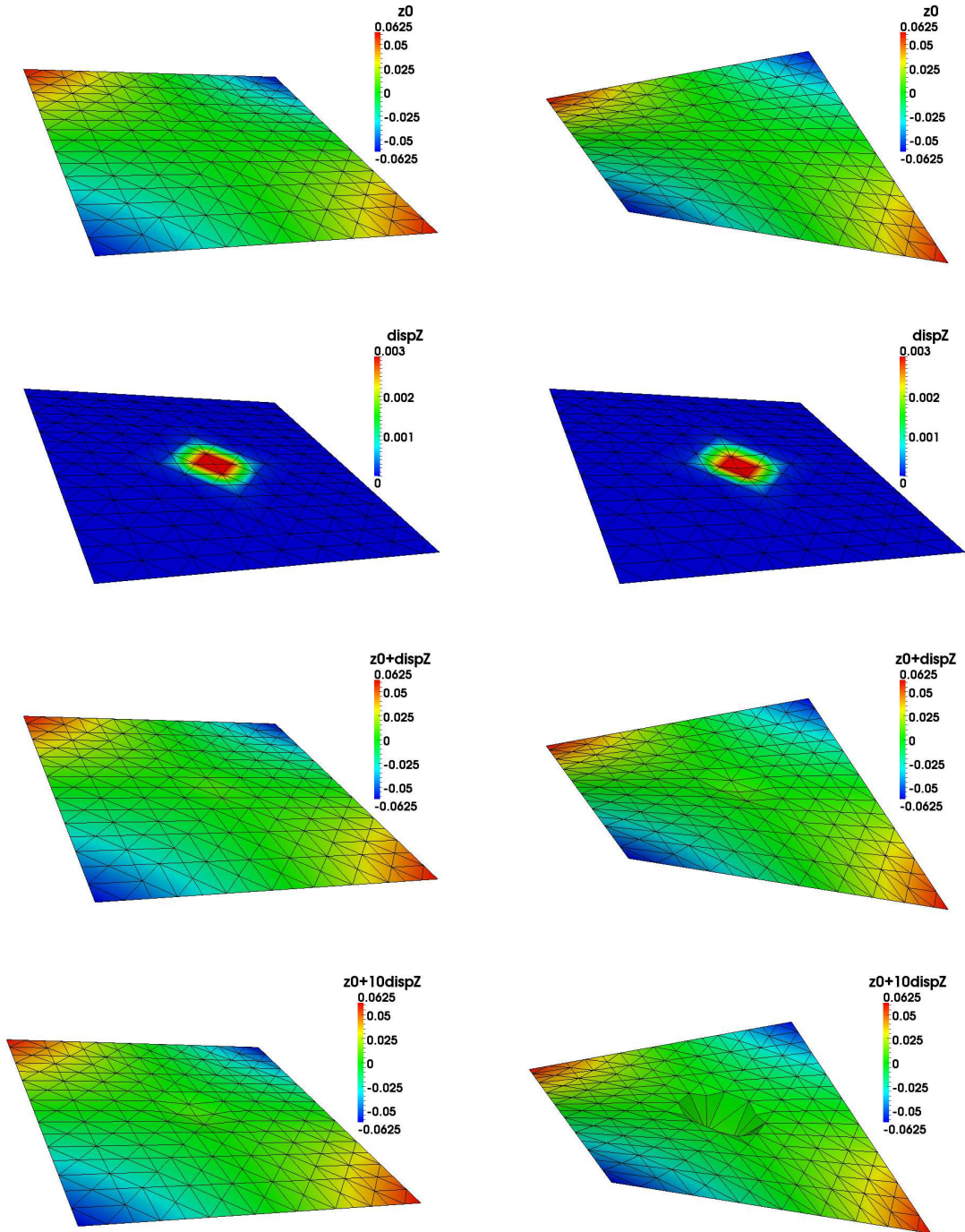


Figure 3: hyper shaped membrane: left column: out-of-plane initial shape z-coordinate in m; out-of-plane z-displacement in m; sum of out-of-plane initial shape z-coordinate and out-of-plane z-displacement in m; sum of out-of-plane initial shape z-coordinate and $10 \times$ out-of-plane z-displacement in m; right column: out-of-plane initial shape z-coordinate in m, z-scale factor 10; out-of-plane z-displacement in m, z-scale factor 10; sum of out-of-plane initial shape z-coordinate and out-of-plane z-displacement in m, z-scale factor 10; sum of out-of-plane initial shape z-coordinate and $10 \times$ out-of-plane z-displacement in m, z-scale factor 10

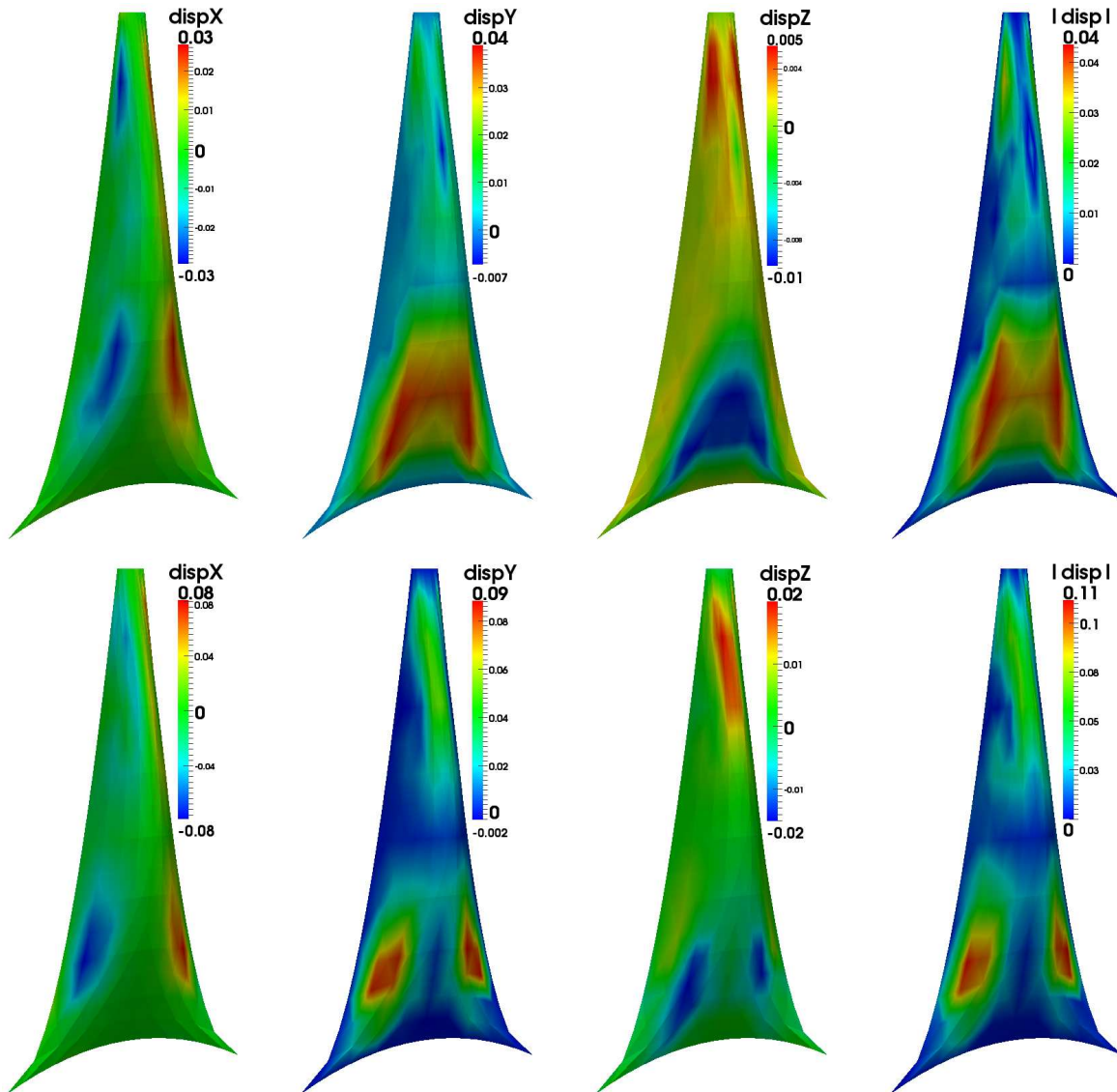


Figure 4: spinnaker sail membrane: top row: cartesian displacement components and displacement magnitude in m for horizontal load of 10 N/m^2 (in y-direction); bottom row: cartesian displacement components and displacement magnitude in m for horizontal load of 100 N/m^2 (in y-direction)